Crystal structure of *Bacillus subtilis* YabJ, a purine regulatory protein and member of the highly conserved YjgF family

Sangita Sinha*, Pekka Rappu†, S. C. Lange*, Pekka Mäntsälä†, Howard Zalkin‡, and Janet L. Smith*§

Departments of *Biological Sciences and ‡Biochemistry, Purdue University, West Lafayette, IN 47907; and †Department of Biochemistry and Food Chemistry, University of Turku, Vatselankatu 2, FIN-20014 Turku, Finland

Communicated by Michael G. Rossmann, Purdue University, West Lafayette, IN, September 20, 1999 (received for review July 15, 1999)

The *yabJ* gene in *Bacillus subtilis* is required for adenine-mediated repression of purine biosynthetic genes *in vivo* and codes for an acid-soluble, 14-kDa protein. The molecular mechanism of YabJ is unknown. YabJ is a member of a large, widely distributed family of proteins of unknown biochemical function. The 1.7-Å crystal structure of YabJ reveals a trimeric organization with extensive buried hydrophobic surface and an internal water-filled cavity. The most important finding in the structure is a deep, narrow cleft between subunits lined with nine side chains that are invariant among the 25 most similar homologs. This conserved site is proposed to be a binding or catalytic site for a ligand or substrate that is common to YabJ and other members of the YER057c/YjgF/UK114 family of proteins.

Purine biosynthesis in *Bacillus subtilis* is regulated by the purine operon repressor gene, *purR*. The *purR* operon consists of *purR* and *yabJ*, an ORF of unknown function. The repressor PurR binds to control regions upstream of the transcription start sites and regulates transcription of *purEKBC (orf)QLFMNHD* in the *pur* operon, of *purR* and *yabJ* in the *purR* operon, and of *purA* (1). PurR binding to control-site DNA is blocked by 5-phosphoribosyl-1-pyrophosphate (PRPP), a central nucleotide metabolite that acts as an inducer of *pur* operon and *purA* transcription. 5-phosphoribosyl-1-pyrophosphate is the starting material for purine biosynthesis. No other metabolite, nucleotide, nucleoside, or nucleotide base is known to affect PurR DNA binding *in vitro* (2).

Recently, *yabJ*, the distal coding sequence in the *purR* operon, was shown to affect PurR function *in vivo* (3). Regulation of transcription of purine biosynthetic genes is sensitive to levels of some nutrients and depends on the interrelated pools of 5-phosphoribosyl-1-pyrophosphate, nucleotides, nucleosides, and nucleotide bases. Adenine uptake by *B. subtilis* indirectly increases PurR repression of *pur* operon and *purA* transcription through changes to the 5-phosphoribosyl-1-pyrophosphate pool. YabJ is also required for adenine-mediated repression of *purA in vivo* (3). The mechanism by which YabJ stimulates adenine-mediated repression of *purA* by PurR is unknown. However, YabJ and PurR may be cotranslated and produced in stoichiometric quantities *in vivo* because the last codon of *purR* overlaps the initiation codon of *yabJ*.

YabJ belongs to a widely distributed family of proteins of unknown function. Members of the YER057c/YjgF/UK114 family of proteins are identified by sequence similarity, having 20–98% pairwise identity. The family is named for genes or proteins in yeast (YER057c), *Escherichia coli* (*yjgF*), and goat (UK114). All are ≈14-kDa proteins and do not occur as domains of larger proteins. Many YjgF proteins are acid-soluble. A variety of biological processes have been reported to be influenced by YjgF proteins, in addition to the YabJ function in purine regulation. Homologs occur in bacteria, animals, and fungi but are absent from the genomes of most archaea and of several parasitic prokaryotes that also lack many biosynthetic pathways. No YjgF homolog has yet been detected in a plant, although its presence in a cyanobacterium (4) suggests that it may also occur in plants. No three-dimensional structures of YjgF proteins have been published, although crystallization of a rat homolog has been reported (5). Here we present the 1.7-Å crystal structure of *B. subtilis* YabJ. The structure reveals a conserved cleft on the protein surface that will aid in elucidation of a function for this family of proteins.

Materials and Methods

Cloning and Overexpression of *yabJ*. The *yabJ* gene was amplified by PCR from chromosomal DNA of a wild-type *B. subtilis* strain. The 446-bp PCR product was confirmed by sequencing and was cloned into a T7 expression vector to produce plasmid pDR1. *E. coli* strain BL21(DE3)/pLysS was transformed with pDR1. Strain BL21(DE3)/pLysS/pDR1 was grown at 37°C in LB medium supplemented with 100 μg/ml ampicillin to an OD_{600} of 0.6, was induced with 0.4 mM isopropyl β-D-thiogalactoside, and was grown for 10 hr at 30°C. Cells were harvested by centrifugation and were resuspended in 50 mM Tris·HCl (pH 8.0), 2 mM EDTA, 10 mM $MgCl_2$, and 10 μg/ml DNase I (5 ml of buffer per gram of wet cells). The cell pellet was frozen at −20°C.

Purification of YabJ. Frozen BL21(DE3)/pLysS/pDR1 cells were thawed and incubated at room temperature for 15 min. The lysate was clarified by centrifugation at 20,000 × *g* for 30 min. All purification steps were performed at room temperature. The lysate soluble fraction was stirred during addition of 70% perchloric acid to a final concentration of 5%. Precipitated proteins were removed by centrifugation at 12,000 × *g* for 15 min. The perchloric acid extract was neutralized with 1.5 volumes of 1 M Tris·HCl (pH 8.0), and the extract was dialyzed against Buffer A (40 mM sodium phosphate buffer, pH 7.4). The ≈95% pure YabJ sample was chromatographed by using the resin Poros HQ/M (PerSeptive Biosystems, Framingham, MA). The column was washed with 5 volumes of Buffer A. YabJ was eluted with 0.2 M NaCl, was dialyzed against Buffer A, and was concentrated by ultrafiltration. N-terminal sequence analysis showed that Met1 was not present in the purified protein. The protein was stored at 4°C or was frozen in small aliquots for long-term storage at −70°C. The overall yield was 120 mg of purified YabJ per liter of *E. coli* culture.

Crystallization and Data Collection. YabJ was crystallized by hanging-drop vapor diffusion from a 1:1 mixture of protein (6.3 mg/ml YabJ in Buffer A) and reservoir (20% polyethylene glycol 4,000/0.45 M ammonium acetate/0.1 M sodium acetate, pH 4.6) solutions. Crystals grew to a maximum size of ≈0.1 × 0.1 × 0.6 mm in 4–5 days and were stabilized in reservoir solution. A Hg derivative

Abbreviation: rmsd, rms deviation.

Data deposition: The atomic coordinate has been deposited in the Protein Data Bank, www.rcsb.org (PDB ID code 1qd9).

§To whom reprint requests should be addressed. E-mail: smithj@purdue.edu.

The publication costs of this article were defrayed in part by page charge payment. This article must therefore be hereby marked "*advertisement*" in accordance with 18 U.S.C. §1734 solely to indicate this fact.

Table 1. Crystallographic summary

Wavelength	λ_1 1.0095 Å	λ_2 1.0087 Å	λ_3 0.9101 Å	λ_4 1.037 Å	$\lambda_3 + \lambda_4$
Data					
Data range (Å)	30–2.2 (2.28–2.20)	30–2.2 (2.28–2.20)	30–2.0 (2.07–2.00)	20–1.7 (1.76–1.70)	30–1.7 (1.76–1.70)
Unique reflections	14,474	14,485	19,335	33,698	35,377
Average multiplicity	7.3	7.3	7.9	4.7	8.7
Completeness (%)	87.0 (53.4)	87.0 (53.2)	88.0 (56.3)	93.3 (95.7)	97.9 (95.6)
R_{sym} (%)*	4.9 (6.6)	5.2 (6.9)	9.7 (5.4)	3.8 (8.9)	5.3 (8.6)
$\langle I/\sigma_1 \rangle$	15.7 (10.9)	15.4 (10.3)	14.2 (8.2)	24.3 (11.7)	22.9 (12.0)
Phasing power†	1.04	1.20	–	0.77	
Refinement					All data
R_{work}‡					16.6%
R_{free}‡					19.7%
$rmsd_{bonds}$					0.011 Å
$rmsd_{angles}$					1.60°
Average B factor					21.6 Å^2
ϕ, ψ outliers					None
rmsd monomers					0.3 Å

Values in parentheses pertain to the outermost shell of data.

*$R_{sym} = \Sigma_{h,i}|I_{h,i} - \langle I_h \rangle|/\Sigma_{h,i} I_{h,i}$.

†Phasing power = $\langle |F_H| \rangle$/rms lack of closure.

‡$R_{factor} = \Sigma_h||F_{obs}| - |F_{calc}||/\Sigma_h|F_{obs}|$. Five percent of the data were used for R_{free}.

was prepared by soaking for 3 hr in 0.5 mM ethyl Hg phosphate in reservoir solution, followed by back soaking for 0.5 hr.

Crystals were cryoprotected by a 3-min soak in 15% polyethylene glycol 400 in reservoir solution and were flash-frozen in a N_2 cold stream at 100 K. Unit cell parameters in space group $P6_5$ are $a = b = 53.3$ Å and $c = 204.9$ Å, which is consistent with either two (V_m = 3.1 Å^3/Da, ≈60% solvent) or three (V_m = 2.0 Å^3/Da, ≈40% solvent) copies of the YabJ polypeptide per asymmetric unit. All data used for structure determination and refinement were collected from a single, Hg-derivatized, frozen crystal. Multiwavelength anomalous diffraction (MAD) data were collected at BioCARS beam line BM14D at the Advanced Photon Source (Argonne National Laboratory). MAD data (λ_1, λ_2, λ_3; Table 1) were recorded on an Q1 CCD detector (Area Detector Systems, Poway, Ca) as two 80° sweeps of data at each wavelength. Resolution was limited by detector size and the 205-Å *c* axis, resulting in incomplete coverage of reciprocal space at the detector edge. Several weeks later, complete, high resolution, 1.7-Å data (λ_4, Table 1) were collected from the same crystal by using BioCARS beam line BM14C at the Advanced Photon Source. The data were recorded on a Mar 345 imaging plate detector (X-ray Research GmbH, Hamburg, Germany) as a single, 80° sweep of data. Data integration and reduction were done by using the HKL package (6). The MAD data set used for phasing was produced by scaling the λ_1, λ_2, and λ_4 data sets to the merged data for λ_3, using SCALEIT from the CCP4 suite (7). For phase and model refinement, a complete high-resolution data set ($\lambda_3 + \lambda_4$, Table 1) was generated by merging data at λ_3 (30–2.5 Å) and λ_4 (3–1.7 Å).

Structure Determination and Refinement. Positions of three Hg atoms were determined by inspection of a Bijvoet difference Patterson map using the λ_2 data set. Refinement of the Hg partial structure and MAD phasing were performed by the pseudo-isomorphous replacement approach using MLPHARE (8). Noncrystallographic 3-fold symmetry was clearly visible in the unmodified MAD map at 2.7-Å resolution. A C3 noncrystallographic symmetry operator was located and refined by using NCS6D (9). Phases were refined and extended to 2.0 Å by 3-fold averaging, histogram matching, and solvent flattening with a 32% solvent mask using DM (10) and the $\lambda_3 + \lambda_4$ data set. The overall figure of merit for all reflections to 2.0 Å was 0.63.

All model building was done in the program O (11). The model was refined against the $\lambda_3 + \lambda_4$ data set using maximum likelihood amplitude and phase probability targets using CNS (12). The initial model had $R_{work} = 0.355$ and $R_{free} = 0.351$ for all data between 30.0 and 2.0 Å. During the initial cycles of refinement, the model was restrained by 3-fold noncrystallographic symmetry. The last iteration of refinement and model building was followed by one round of atomic occupancy refinement for residues in dual positions and for the ethyl Hg ions. Final $R_{work} = 0.166$ and $R_{free} = 0.197$ for all data between 30.0 and 1.7 Å. The model, including 124 residues in each of three YabJ monomers, one ethyl Hg ion covalently linked to Cys104 in each of two monomers, two partially occupied Hg sites in the third monomer, six acetate ions, and 474 water molecules, has been deposited in the Protein Data Bank and is available with ID code 1qd9. A crystallographic summary is presented in Table 1.

Results and Discussion

Protein Production and Structure Determination. *B. subtilis* YabJ was readily produced in *E. coli* from an inducible plasmid. Purification was simplified by the acid extraction step. We tried this approach because several YabJ homologs were reported to be acid stable (13, 14), and acid solubility was exploited in the purification of the rat homolog (15), which is 45% identical to YabJ. The crystal structure was determined by Hg MAD, based on modification of the single cysteine residue in YabJ. A complete, high-quality model of YabJ resulted from refinement against complete 1.7-Å data. Electron density is clear for all parts of the protein. The model agrees well with the diffraction data and with stereochemical criteria (Table 1). No residues are in forbidden regions of the Ramachandran plot (16). The estimated coordinate error of the final model is 0.19 Å (17).

Protein Structure. The YabJ monomer is a 124-residue polypeptide folded into a single domain. The YabJ fold is a six-stranded, mostly antiparallel β-sheet with one parallel connection (Fig. 1). Two α-helices pack against one face of the β-sheet. The core of each monomer includes no ionizable groups or polar side-chain inter-

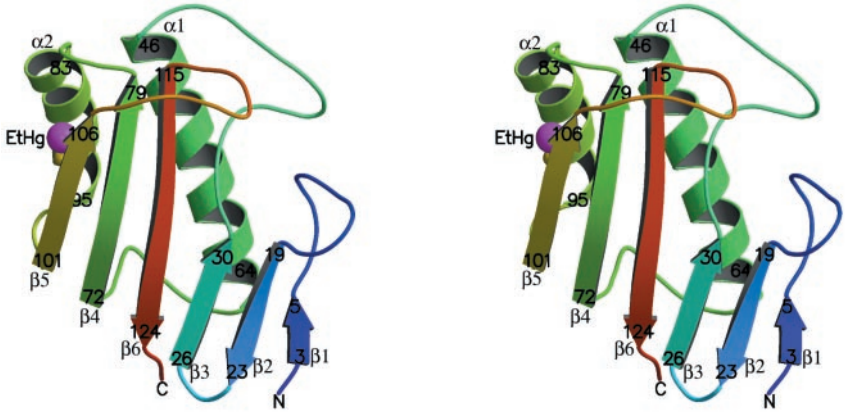

Fig. 1. Stereo view of the YabJ monomer. The ribbon diagram is rendered in rainbow colors from blue at the N terminus to red at the C-terminus. The figure was produced with MOLSCRIPT (31) and RASTER3D (32).

actions. This structural feature may contribute to the acid stability of YabJ. Preliminary refinement of the YabJ model against data from Hg-free crystals at pH 6.5 indicates no significant structural change from the Hg complex at pH 4.6 apart from rotation of the Cys104 side chain from $\chi_1 = 180°$ to $\chi_1 = -60°$.

YabJ is a symmetric trimer in crystals (Fig. 2). The three β-sheets of the trimer form a triangular barrel, with the β-strands approximately parallel to the barrel 3-fold axis. The six α-helices of the trimer pack on the outside of the barrel. Residues in strands $\beta3$–$\beta6$ of each monomer participate in the trimer interface, which is constructed of alternating hydrophobic and polar regions. At the top of the barrel, the three backbones form a ring of nine intersubunit hydrogen bonds involving residues 106, 108, and 109. Below this polar region is an extensive hydrophobic interface including six residues from each monomer (Phe77, Met81, Val105, Val107, Leu110, Pro111). In the center of the trimer is a polar cavity filled with 21 ordered water molecules and ringed with six intersubunit polar contacts, consisting of a salt bridge from Lys73 ($\beta4$) and a hydrogen bond from Ser103 ($\beta5$) in each monomer to Glu119 ($\beta6$) in an adjacent monomer. Each water molecule in the cavity forms at least three hydrogen bonds to other waters or to protein atoms (Tyr28, Ser29, Lys73, Thr75, Glu119, Val120), and the constellation of 21 waters has ≈3-fold symmetry. Another 12 intersubunit hydrogen bonds are formed by nearby residues (Ser18, Ser30, and Gly31 with Lys99, Pro100, and Arg102). The floor of the polar cavity is formed by three Tyr28 ($\beta3$) side chains, which are hydrogen-bonded to a cavity water molecule. The cavity waters would be accessible to external bulk solvent by slight conformational breathing of the Tyr28 side chains. The Tyr28 residues are the beginning of another hydrophobic interface, which includes eight residues from each monomer (Ile21, Val23, Met26, Tyr28, Val72, Ala101, Ile121, Leu123). At the bottom of the barrel is a ring of six hydrogen bonds between the amides of Asn24 and Asn25 in adjacent subunits.

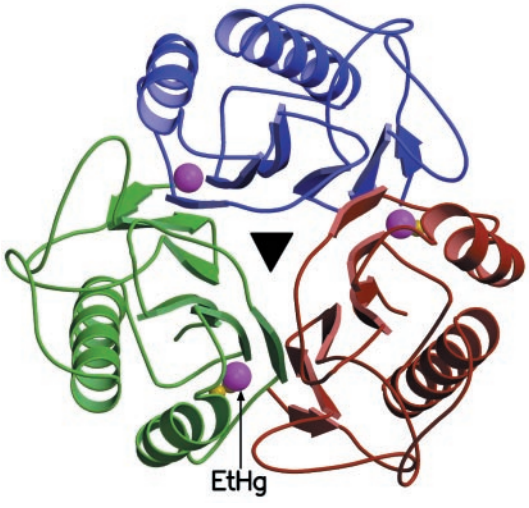

Fig. 2. YabJ Trimer. Subunits are rendered in different colors in this ribbon diagram viewed along the molecular threefold axis. The position of the Hg ion used to solve the structure and bound to Cys104 is indicated with a sphere.

The YabJ quaternary structure has not been established in solution. Several features of the crystalline trimer, including the extent and character of buried monomer surface and the dehydration of subunit interfaces, are consistent with a YabJ trimer in solution. The total monomer-accessible surface buried in the trimer is very large, a total of 1,850 Å^2, ≈28% of the total (18). Two extensive hydrophobic contact regions are part of the trimeric aggregate. Apart from the central cavity described above, the subunit interfaces do not bury any water molecules. Thus, the subunit interfaces of the crystalline trimer are much more like biological aggregates than like crystal contacts, which are extensively hydrated, rather small and very polar. Some YabJ homologs have been reported to be dimeric (13, 19, 20, 29). However, residues forming the polar and hydrophobic zones of the subunit interface are very well conserved among the YabJ homologs, suggesting that all are trimers.

Neighboring subunits of the trimer create three clefts on the outer surface of YabJ. The clefts are narrow (8–9 Å) and deep (12–13 Å). Glu117 forms the innermost surface of each cleft, and several hydrophobic side chains ring the outermost surface.

YabJ in the *purR* operon of *B. subtilis*. Transcription of *purA* is repressed ≈10-fold *in vivo* by addition of adenine to cells (3). This repression is mediated by PurR. However, disruption of YabJ results in the loss of adenine-mediated PurR repression by an unknown mechanism. The predominance of acidic residues on the surface of YabJ (calculated pI = 5.3) suggests that it does not interact directly with DNA. Preliminary soaking experiments with YabJ crystals and various purine-containing molecules and calcium ions, which are reported to bind a YabJ homolog (20), have not resulted in binding in the cleft or anywhere else on YabJ. Further experiments are underway to identify a ligand or substrate.

Stuctural Homolog. YabJ has no detectable sequence similarity to any other protein in the structure database (21). Unexpectedly, it has a fold (22) and aggregation state in common with chorismate

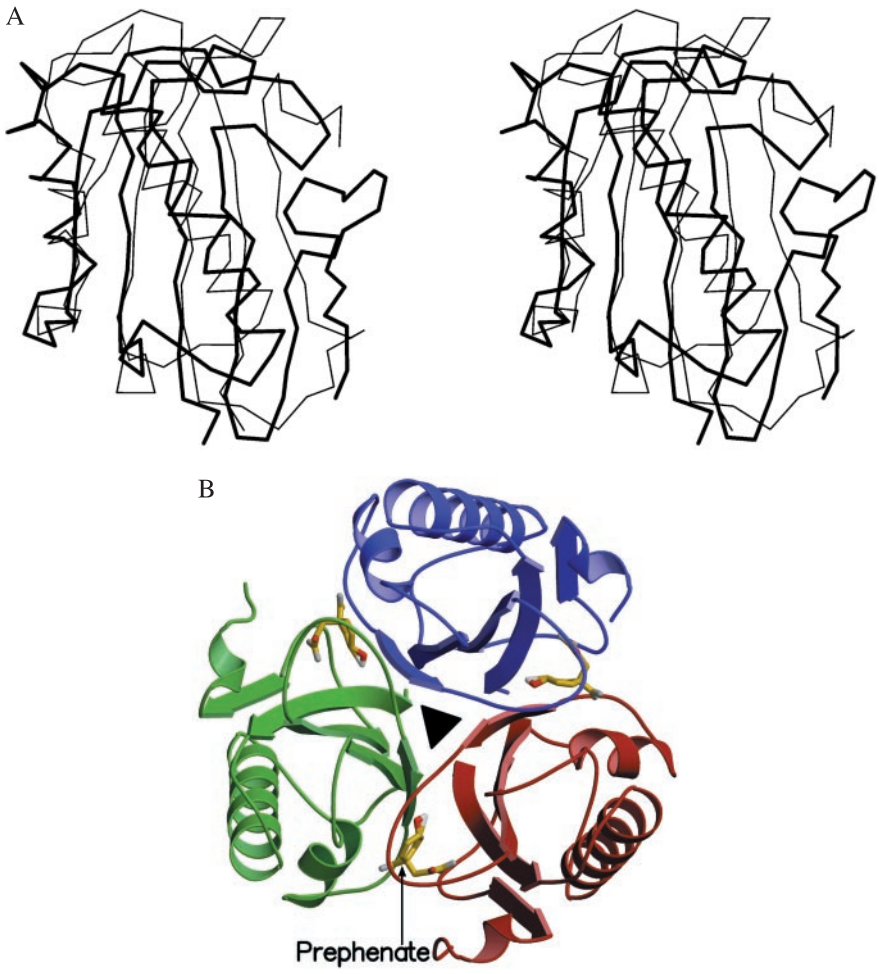

Fig. 3. Comparison of YabJ and *B. subtilis* chorismate mutase. (*A*) Superposition of subunits. C_α traces of YabJ (thick lines) and chorismate mutase (thin lines) are overlaid. Orientation is similar to Fig. 1. (*B*) Ribbon diagram of the chorismate mutase trimer. The reaction product prephenate is shown in the active site cleft. Orientation is as in Fig. 2.

mutase from *B. subtilis* (23). The core fold, β3–β6 and α1, is present in both structures. The second α-helix of YabJ is replaced by a shorter 3_{10}-helix in chorismate mutase. Strands β1 and β2 of YabJ and a fifth, C-terminal strand of chorismate mutase lie on the same end of the core β-sheet but are not superimposable. Based on the structure alignment, the sequences of YabJ and chorismate mutase are only 8% identical. The rmsd for the 83 superimposable C_α atoms per monomer is 2.6 Å (Fig. 3*A*). YabJ and chorismate mutase also form very similar trimers with an rmsd of 3.3 Å for 249 C_α atoms. However, the trimer interface of chorismate mutase is entirely hydrophobic and lacks the polar central cavity of YabJ.

Chorismate mutase catalyses the unimolecular, pericyclic rearrangement of chorismate to prephenate, a reaction at the branch point of the biosynthetic pathway for aromatic amino acids. The three active sites of the chorismate mutase trimer are located in clefts between subunits, analogous to the clefts at the subunit interfaces of the YabJ trimer (Fig. 3*B*). Eleven residues in the active site of chorismate mutase have been implicated in substrate binding and transition state stabilization (23). Two of these side chains, Phe 57 and Cys 75, have chemical and topological equivalents, Phe 84 and Cys 104, in YabJ. However, elsewhere in the cleft, YabJ and chorismate mutase do not have common functional groups. We conclude that YabJ and chorismate mutase probably have a common ancestor but have evolved to perform different functions.

Sequence Homologs. YabJ belongs to the YER057c/YjgF/UK114 family of small proteins (ProSite accession nos. PS01094 and UPF0076). We identified a total of 37 homologs having 20–53% sequence identity with YabJ in the sequence database (21). This level of identity indicates a common ancestor, a common fold, and possibly a common function for the proteins.

No invariant residues result from multiple alignment (24) of the 38 sequences of YabJ and its homologs. However, if the homologs have evolved to more than one function, invariance would not be expected. To probe the sequence data for clues to biochemical function, we looked for a subset of more closely related sequences. Based on the multiple sequence alignment, the homologs were divided into two groups—a "high identity" group of 25 more closely related sequences, each having at least 43% identity with another sequence in the group, and a "low identity" group of 13 more divergent sequences, each having generally <30% identity to any member of either group. The high-identity group, including YabJ, has nine invariant residues (Fig. 4). Although they are spread throughout the primary sequence, all of these residues map to the narrow, deep cleft between subunits of the YabJ trimer (Fig. 5). This site is structurally analogous to the active site of chorismate mutase. The clustering of invariant residues in the cleft strongly suggests a common molecular function of catalysis or binding for members of the high-identity group.

Two structural databases were queried for similar residue constellations in YabJ and any protein of known structure and function. PROCAT (25) is a database of functional groups in enzyme active

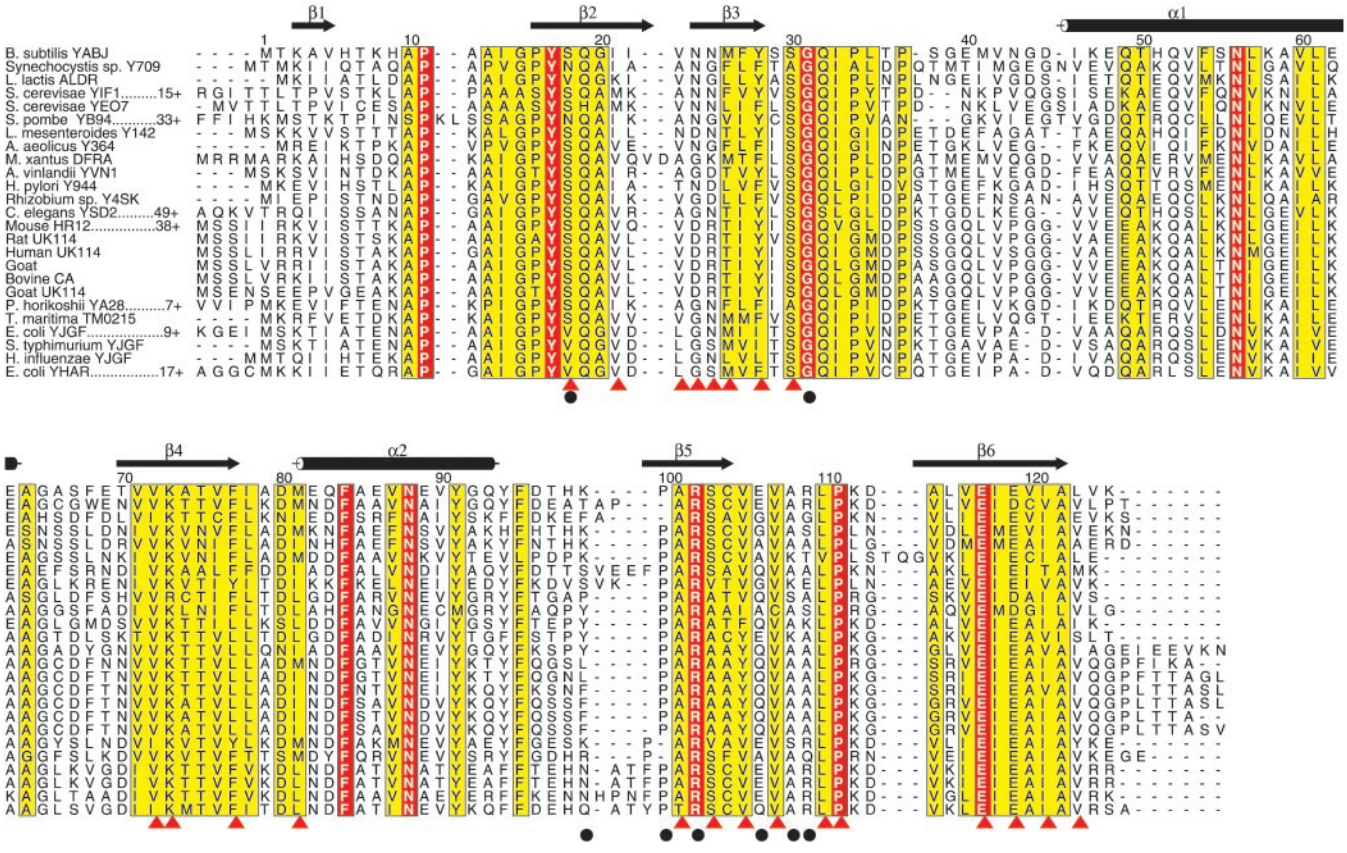

Fig. 4. Comparison of sequences of YabJ and 24 homologs in the high-identity group. Residues in red boxes are invariant; in yellow boxes are sites of conservative substitution. Secondary structures are indicated above the alignment. Residues in the subunit interface are indicated by triangles below the alignment, and those with main-chain interactions by circles. Multiple sequence alignment was done with CLUSTALW (24). The figure was produced with ALSCRIPT (33).

sites. None of these active site templates matches any constellation of residues in the YabJ structure. Conversely, the nine YabJ side chains that are invariant in the high-identity group do not have an analog among protein structures deposited in the Protein Data Bank, as probed with the program SPASM (26). Thus, it appears that the arrangement of residues in the conserved cleft of YabJ does not exist in any reported protein structure.

Biological functions attributed to YabJ homologs do not point to a common biochemical activity. Most of the homologs are hypothetical proteins of unknown function. The genetic context of *yabJ* (*purR* operon) correlates with the observed phenotype of *yabJ*$^{-}$ (loss of *purA* repression by adenine). Similarly, *Lactococcus lactis aldR* has been implicated in regulation of isoleucine biosynthesis (27). *Salmonella typhimurium yjgF* may have a role in regulation of the isoleucine and thiamine biosynthetic pathways (28). In cases in which protein products have been studied, no certain biochemical activity has been identified, and a wide variety of biological functions has been proposed. The rat and human homologs are

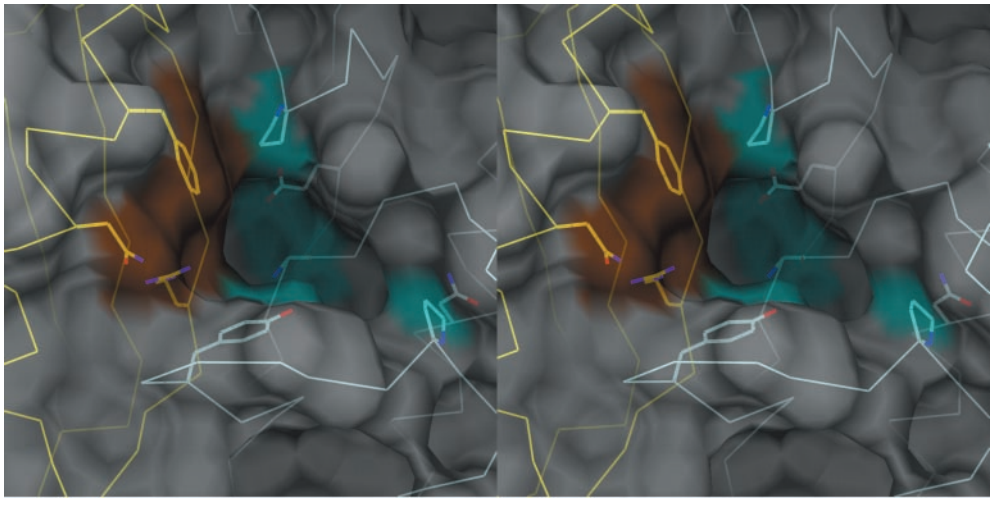

Fig. 5. Stereo view of the intersubunit cleft of YabJ. The translucent molecular surface is in gray, with surfaces of invariant residues from the two subunits in rust and cyan. C_α wire diagrams for two subunits are yellow and white, as are the side chains of invariant residues (Phe84, Asn88, and Arg102 in the yellow subunit, and Pro11, Tyr17, Gly31, Asn56, Pro111, and Glu117 in the white subunit). The figure was produced with DINO (ref. 34; http://www.bioz.unibas.ch/~x-ray/dino).

putative translation inhibitors (14, 29), goat UK114 is implicated in tumor antigenicity (30), mouse Hrp12 is thought to be a heat response protein (19), and the bovine and rat homologs are proposed to affect activation of the calcium-dependent protease calpain (20). Sequences for all of these homologs are in the high-identity group. The strong conservation of side chains in the YabJ cleft implies that the homologs of the high-identity group achieve their variety of biological functions by a common biochemical mechanism.

Any common biochemical mechanism for the broadly distributed YabJ homologs would necessarily involve ligand or substrate binding to the 12-Å deep, 8-Å wide conserved cleft at the subunit interface (Fig. 5). We screened broadly for a small-molecule ligand by soaking crystals at neutral pH in a stabilizing solution augmented with *B. subtilis* cell extract. No electron density for a ligand was identified in difference electron density maps computed by using diffraction data from the soaked crystals. This negative result does not distract us from investigation of the conserved cleft. Studies are underway to identify a ligand or substrate in solution and *in vivo*.

We propose that YabJ and the high-identity homologs use the conserved, deep, narrow cleft for catalysis or binding of a common chemical entity. Molecular mechanisms by which these proteins could use a common biochemistry to influence a variety of biological processes include, among others, binding a regulatory macromolecule, altering the concentration of a key small-molecule metabolite through catalysis, and binding another macromolecule after a ligand-induced conformational change. Use of the conserved, deep, narrow cleft for binding implies recognition of an appropriately shaped small-molecule ligand or a single amino acid residue in a protein ligand. The structure of YabJ should be an important guide for identification of this molecule. This work also illustrates the challenges of deducing protein function from sequence and three-dimensional structure.

Note. After completion of this manuscript, a structure of *E. coli* YjgF, a YabJ homolog, was presented at the annual meeting of the American Crystallographic Association (35). The function of *E. coli* YjgF is unknown. In *E. coli*, *yjgF* is not linked to *purR*, and *E. coli purR* is unrelated to *B. subtilis purR*.

The authors thank the staff of BioCARS at the Advanced Photon Source, Argonne National Laboratory, for their advice during the data collection and Carol Greski for expert preparation of the manuscript. This work was supported by National Institutes of Health Grants DK-42303 to J.L.S. and GM-24658 to H.Z. and by the Finnish Ministry of Education (P.M.).

1. Weng, I., Nagy, P. & Zalkin, H. (1995) *Proc. Natl. Acad. Sci. USA* **92,** 7455–7459.
2. Shin, B. S., Stein, A. & Zalkin, H. (1997) *J. Bacteriol.* **179,** 7394–7402.
3. Rappu, P., Shin, B. S., Zalkin, H. & Mäntsälä, P. (1999) *J. Bacteriol.* **181,** 3810–3815.
4. Chavez, S., Reyes, J. C., Chauvat, F., Florencio, F. J. & Candau, P. (1995) *Plant Mol. Biol.* **28,** 173–188.
5. Djinovíc Carugo, K., Saraste, M. & Oka, T. (1999) *Acta Crystallogr. D* **55,** 667–668.
6. Otwinowski, Z. & Minor, W. (1997) *Methods Enzymol.* **276,** 307–326.
7. Collaborative Computational Project Number 4 (1994) *Acta Crystallogr. D* **50,** 760–763.
8. Otwinowski, Z. (1991) in *Isomorphous Replacement and Anomalous Scattering*, eds. Wolf, W., Evans, P. R. & Leslie, A. G. W., (Science and Engineering Research Council, Daresbury, U.K.), pp. 80–86.
9. Kleywegt, G. J. & Jones, T. A. (1997) *Acta Crystallogr. D* **53,** 179–185.
10. Cowtan, K. D. (1994) *Joint CCP4 and ESF-EACBM Newsletter on Protein Crystallography* **31,** 34–38.
11. Jones, T. A., Zou, J.-Y., Cowan, S. W. & Kjeldgaard, M. (1991) *Acta Crystallogr. A* **47,** 110–119.
12. Brünger, A. T., Adams, P. D., Clore, G. M., DeLano, W. L., Gros, P., Grosse-Kunstleve, R. W., Jiang, J.-S., Kuszewski, J., Nilges, M., Pannu, N. S., *et al.* (1998) *Acta Crystallogr. D* **54,** 905–921.
13. Levy-Favatier, F., Cuisset, L., Nedelec, B., Tichonichy, L., Kruh, J. & Delpech, M. (1993) *Eur. J. Biochem.* **212,** 665–673.
14. Schmiedeknecht, G., Kerkhoff, C., Orso, E., Stohr, J., Aslanidis, C., Nagy, G. M., Knuechel, R. & Schmitz, G. (1996) *Eur. J. Biochem.* **242,** 339–351.
15. Oka, T., Nishimoto, Y., Sasagawa, T., Kanouchi, H., Kawasaki, Y. & Natori, Y. (1999) *Cell. Mol. Life Sci.* **55,** 131–134.
16. Laskowski, R. A., MacArthur, M. W., Moss, D. S. & Thornton, J. M. (1993) *J. Appl. Crystallogr.* **26,** 283–291.
17. Read, R. J. (1986) *Acta Crystallogr. A* **42,** 140–149.
18. Nicholls, A., Sharp, K. & Honig, B. (1991) *Proteins* **11,** 281–296.
19. Samuel, S. J., Tzung, S. P. & Cohen, S. A. (1997) *Hepatology* **25,** 1213–1222.
20. Melloni, E., Michetti, M., Salamino, F. & Pontremoli, S. (1998) *J. Biol. Chem.* **273,** 12827–12831.
21. Altschul, S. F., Gish, W., Miller, W., Myers, E. W. & Lipman, D. J. (1990) *J. Mol. Biol.* **215,** 403–410.
22. Holm, L. & Sander, C. (1993) *J. Mol. Biol.* **233,** 123–138.
23. Chook, Y. M., Gray, J. V., Ke, H. & Lipscomb, W. N. (1994) *J. Mol. Biol.* **240,** 476–500.
24. Thompson, J. D., Higgins, D. G. & Gibson, T. J. (1994) *Nucleic Acids Res.* **22,** 4673–4680.
25. Wallace, A. C., Borkakoti, N. & Thornton, J. M. (1997) *Protein Sci.* **6,** 2308–2323.
26. Kleywegt, G. J. (1999) *J. Mol. Biol.* **285,** 1887–1897.
27. Goupil-Feuillerat, N., Cocaign-Bousquet, M., Godon, J. J., Ehrlich, S. D. & Renault, P. (1997) *J. Bacteriol.* **179,** 6285–6293.
28. Enos-Berlage, J. L., Langendorf, M. J. & Downs, D. M. (1998) *J. Bacteriol.* **180,** 6519–6528.
29. Oka, T., Tsuji, H., Noda, C., Sakai, K., Hong, Y., Suzuki, I., Muñoz, S. & Natori, Y. (1995) *J. Biol. Chem.* **270,** 30060–30067.
30. Ceciliani, F., Faotto, L., Negri, A., Colombo, I., Berra, B., Bartorelli, A. & Ronchi, S. (1996) *FEBS Lett.* **393,** 147–150.
31. Kraulis, P. J. (1991) *J. Appl. Crystallogr.* **24,** 946–950.
32. Merritt, E. A. & Bacon, D. J. (1997) *Methods Enzymol.* **277,** 505–524.
33. Barton, G. L. (1993) *Protein Eng.* **6,** 37–40.
34. Sanner, M. F., Olson, A. J. & Spehner, J. (1995) *Proc. 11th Assoc. Comput. Machinery Symp. Comput. Geom.*, C6–C7.
35. Volz, K. (1999) *Protein Sci.*, in press.